A study on ground truth data for impact damaged polymer matrix composites

Sarah M. Wallentine, and Michael D. Uchic

Citation: AIP Conference Proceedings **1949**, 120002 (2018); doi: 10.1063/1.5031589
View online: https://doi.org/10.1063/1.5031589
View Table of Contents: http://aip.scitation.org/toc/apc/1949/1
Published by the American Institute of Physics

A Study on Ground Truth Data for Impact Damaged Polymer Matrix Composites

Sarah M. Wallentine[1, a)] and Michael D. Uchic[, 1, b)]

[1]*Materials State Awareness Branch, Structural Materials Division*
Materials and Manufacturing Directorate, Air Force Research
Laboratory Wright-Patterson Air Force Base, Ohio, USA

[a)]Corresponding author: sarah.wallentine.1@us.af.mil
[b)]michael.uchic@us.af.mil

Abstract. This study presents initial results toward correlative characterization of barely-visible impact damage (BVID) in unidirectional carbon fiber reinforced polymer matrix composite laminate plates using nondestructive ultrasonic testing (UT) and destructive serial sectioning microscopy. To produce damage consistent with BVID, plates were impacted using an instrumented drop-weight tower with pneumatic anti-rebound brake. High-resolution, normal-incidence, single-sided, pulse-echo, immersion UT scans were performed to verify and map internal damage after impact testing. UT C-scans were registered to optical images of the specimen via landmark registration and the use of an affine transformation, allowing location of internal damage in reference to the overall plate and enabling specimen preparation for subsequent serial sectioning. The impact-damaged region was extracted from each plate, prepared and mounted for materialographic sectioning. A modified RoboMet.3D version 2 was employed for serial sectioning and optical microscopy characterization of the impact damaged regions. Automated montage capture of sub-micron resolution, bright-field reflection, 12-bit monochrome optical images was performed over the entire specimen cross-section. These optical images were post-processed to produce 3D data sets, including segmentation to improve visualization of damage features. Impact-induced delaminations were analyzed and characterized using both serial sectioning and ultrasonic methods. Those results and conclusions are presented, as well as future direction of the current study.

INTRODUCTION

Over the past several decades, polymer-matrix composite (PMC) materials have proliferated as secondary and primary components in civil and military aircraft structures. High strength-to-weight ratios are a key benefit of structural composites; however, there is incomplete understanding and predictive capability of damage formation and growth in these materials. Thus, a significant amount of conservatism must be designed into components and structures, and potential weight savings are not fully realized in practice. Current Air Force Research Laboratory (AFRL) efforts are focused on the maturation of capabilities to enable a life management framework for composites, aligned with damage tolerance via fracture mechanics approach used for metallic structures [1]. In parallel with ongoing development of damage evolution modeling for PMCs [2], AFRL is developing nondestructive evaluation (NDE) methods suitable for field/Depot inspection environments that are capable of three-dimensional (3D) characterization of damage in PMCs. Specifically, recent work has been focused on 3D characterization of sub-surface morphology of impact-damaged PMCs [3] via an integrated program of normal- and oblique-angle ultrasonic experiments combined with model-based inversion to interpret the ultrasonic data. Although this program is still at an early stage of development, it has been recognized that the need exists for eventual independent verification of these methods. This study examines the viability of one approach for independent verification of the size, shape, and interconnectivity of impact damage within PMCs.

One method for generating high-resolution, large volume microstructural data is through the use of serial sectioning experiments [4]. An automated multi-modal serial sectioning system called LEROY has been successfully

44th Annual Review of Progress in Quantitative Nondestructive Evaluation, Volume 37
AIP Conf. Proc. 1949, 120002-1–120002-10; https://doi.org/10.1063/1.5031589
Published by AIP Publishing. 978-0-7354-1644-4/$30.00

developed and implemented for multi-scale microstructural characterization of engineering materials at AFRL, which utilizes a RoboMet.3D system for mechanical grinding and polishing to perform sequential material removal. Concurrently, an open-source software environment that addresses the needs for quantitative digital analysis of microstructural data called DREAM.3D (Digital Representation Environment for the Analysis of Microstructure in 3D) has also been developed via AFRL-funded research [5]. The combined use of these technologies has successfully provided 3D visualization and quantification of manufacturing defects within PMC laboratory samples, as shown pictorially in Fig. 1a. A subset of this data was successfully imported and modeled in the PZFlex modeling suite (Fig. 1b), which demonstrated one potential pathway to utilize 3D microstructural information within forward modeling software that simulates ultrasonic inspection. A future goal is to repeat this demonstration for PMC samples that contain impact damage.

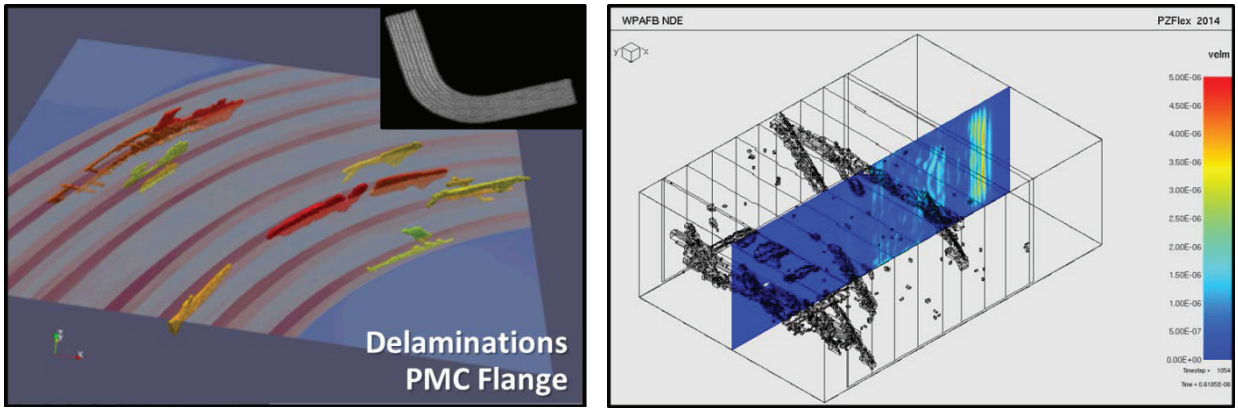

(a) (b)

FIGURE 1. RoboMet.3D → DREAM.3D → PZFlex data pipeline proof-of-concept. (a) Characterization of manufacturing defects in a PMC laminate. (b) Representation of data subset in PZFlex ultrasonic modeling suite.

It is hypothesized that mechanical polishing-based serial sectioning in conjunction with optical microscopy will provide high fidelity, ground truth data of impact damage in aerospace grade PMC structures, to enable independent verification of inverse NDE models for 3D characterization of impact damage. This paper presents a proof-of-concept study to demonstrate the ability to characterize microscale damage in 3D from a quasi-isotropic PMC panel subjected to low energy impact (< 5 J). An impact-damaged PMC panel was first characterized with nondestructive immersion ultrasound to identify the spatial extent and position of the subsurface delaminations, which was followed by destructive serial sectioning characterization using a modified RoboMet.3D system. For this study, the impact damage features of primary interest are delaminations and transverse matrix cracks.

EXPERIMENTAL PROCEDURES

Materials

The experimental work performed for this study focused on the characterization of impact damage in PMC plates. The PMC plates were fabricated of unidirectional carbon fiber reinforced polymer tape in a $[-45/90/45/0]_{3S}$ quasi-isotropic stacking sequence. The plates were cured in an autoclave as large panels that were 24 x 24 in. (610 x 610 mm). The cured panels have a nominal 1/8 in. (3.2 mm) thickness. Post-cure, the panels were cut for drop-weight impact testing using a waterjet to 6 x 4 in. (152 x 102 mm) plates, per ASTM 7136 [6]. Ultrasonic testing (UT) was performed to verify the absence of manufacturing defects before drop-weight testing.

Generation and Ultrasonic Inspection of Impact Damage

Impact damage was generated in two composite plates using an instrumented drop-weight tower. Each composite plate was clamped with four rubber-ended push clamps in a 5 x 3 in. (127 x 76 mm) open rectangular frame fixture, per ASTM 7136. The fixture was secured to the test stand (Fig. 2), and a 5/8 in. (16 mm) hemispherical striker tip

was used as an impactor in the drop-weight tower. Impact energies associated with initiation of barely visible impact damage (i.e., "damage threshold load") were informed by the work of Flores and Schoeppner [7,8]. Table 1 lists the key parameters of each drop test, as well as the alphanumeric specimen identifier by which each composite specimen will be referred to in this paper.

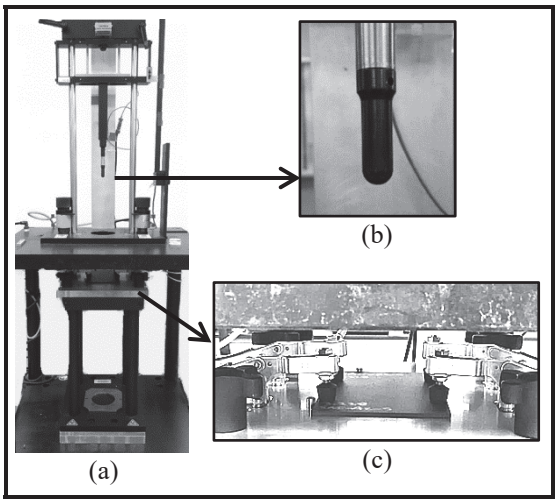

FIGURE 2. (a) Drop-weight impact tower outfitted with (b) a 5/8 in. hemispherical striker tip and (c) rubber-ended push clamp frame fixture.

TABLE 1. Drop-weight impact test set-up and measured parameters

Specimen ID	Drop height (in | m)	Mass (lb | kg)	Velocity (ft/s | m/s)	Energy (ft-lb | J)
D3-5	8.25 | 0.21	2.1 | 4.6	6.57 | 2.00	3.13 | 4.25
D3-6	12.0 | 0.30	2.9 | 1.3	7.89 | 2.40	2.01 | 2.72

After completion of each impact test, UT was performed to characterize damage in the specimens. Hand probe surveys on each specimen indicated damage in proximity to the impact site, using a Panametrics Epoch III Ultrasonic Pulse Receiver with a water-coupled, 5 MHz, 0.75 inch diameter transducer. The approximate area where damage indications were observed was localized and annotated. To enable subsequent data registration between high resolution UT and serial sectioning experiments, copper tape was applied to the PMC sample to create a border around the estimated damage area. A digital camera was used to photograph each specimen (Fig. 3) before performing high resolution UT scans to aid in preparing the samples for correlative serial sectioning characterization.

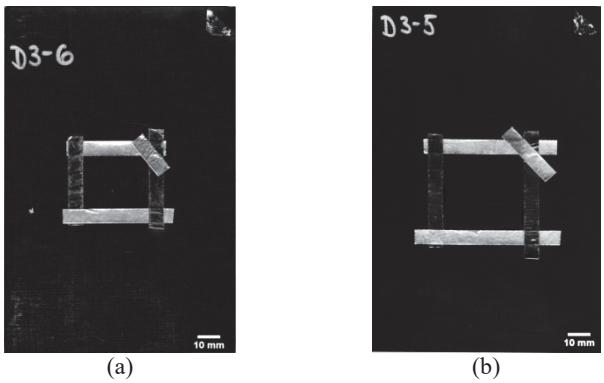

FIGURE 3. Optical images of specimens (a) D3-6 and (b) D3-5. Copper tape surrounds the impact damage area.

High-Resolution Ultrasonic Scans

High-resolution UT was performed using an AFRL/RXCA-developed Material Property Scanning System II (MaPSS II). The three-axis scanning system employs a Panametrics 5900 Pulser/Receiver with gain and attenuation control, 8-bit digitizer, and was configured for normal-incidence, pulse-echo, immersion UT.

Before each scan, the scanning stage was leveled and the probe was also focused and leveled. Scan parameters for each transducer and scan are shown in Table 2. Two UT scans were performed for each specimen, one with each of two transducer frequencies: 50 MHz and 5 MHz. The 50 MHz PVDF probe was employed for improved time (through-thickness) resolution, while the 5 MHz probe was employed to reduce signal noise induced by higher frequencies. In-plane spatial resolution was set by the scan step size of 0.004 in. (0.1 mm) per step. Figure 4 shows representative amplitude C-scans with backwall gate of each specimen and transducer combination.

TABLE 2. Ultrasonic scan parameters

Specimen ID	Transducer			Scan				
	Freq. (MHz)	Diameter (in | mm)	Focal length (in | mm)	Scan area (in | mm)	Step size (in | mm)	A-Scan length (μs)	Sample rate (μs)	Samples per A-Scan
D3-5	50	0.5 | 12.7	0.5 | 12.7	0.22 x 0.22 | 56 x 56	0.004 | 0.1	4.096	0.004	1024
	5	0.25 | 6.35	0.75 | 19.05	0.22 x 0.22 | 56 x 56	0.004 | 0.1	5.12	0.004	1280
D3-6	50	0.5 | 12.7	0.5 | 12.7	0.20 x 0.21 | 50 x 54	0.004 | 0.1	4.096	0.004	1024
	5	0.25 | 6.35	0.75 | 19.05	0.17 x 0.19 | 44 x 48	0.004 | 0.1	5.12	0.004	1280

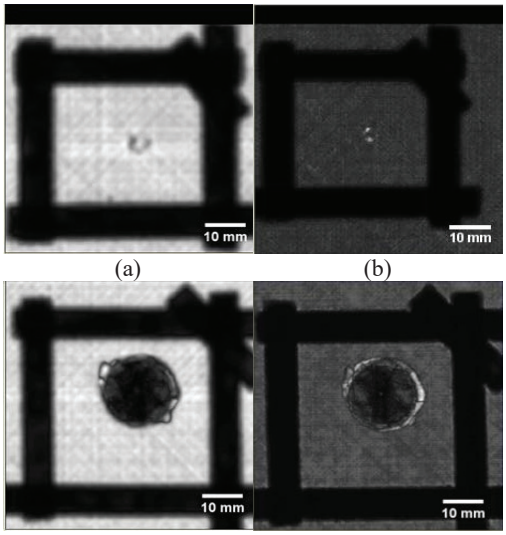

FIGURE 4. Amplitude C-Scans with backwall gate of low-energy impacted specimen D3-6 with: (a) 5 MHz and (b) 50 MHz transducers; and higher-energy impacted specimen D3-5 with: (c) 5 MHz and (d) 50 MHz transducers.

High-resolution UT scans served two purposes for this study. The first purpose was for use in locating the damaged region within each specimen with respect to the overall specimen geometry. This nondestructive characterization of the damage "footprint" was essential as the internal damage is otherwise unobservable. For each specimen, registration of the optical image to the 50 MHz UT C-scan was performed to establish damage location, thus enabling sample preparation for subsequent serial sectioning (Fig. 5). Spatial registration of UT and optical data was accomplished via landmark registration and the use of an affine transformation of the resultant images from each source.

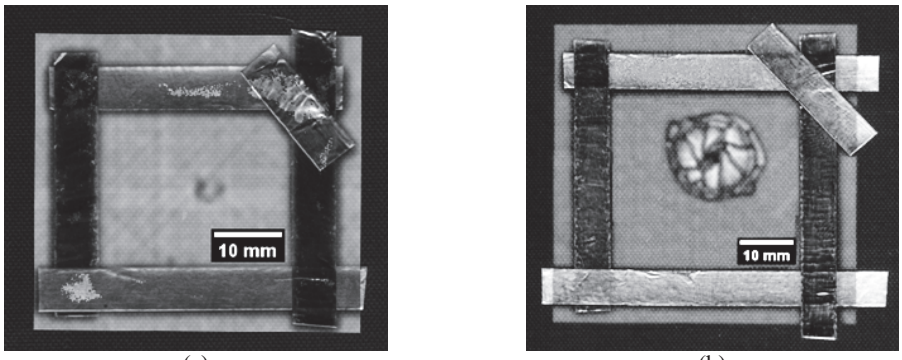

(a) (b)

FIGURE 5. Registration of 50 MHz UT C-scan to optical image of (a) low-energy impacted specimen D3-6 and (b) higher-energy impacted specimen D3-5.

Secondly, the high-resolution UT scans were used for correlative analysis of damage characterization between nondestructive ultrasound and destructive serial sectioning. Due to the limitations of normal-incidence pulse-echo UT scans, not all damage features were able to be correlated between the two modalities. For example, normal-incidence UT responds well to inter-ply delaminations, but has minimal signal response to other damage morphologies such as transverse matrix cracks. Therefore, the analysis presented in this study was limited to inter-ply delaminations.

Automated Serial Sectioning and Optical Microscopy Characterization

A modified RoboMet.3D version 2 was employed for serial sectioning and optical microscopy characterization of the impact damaged regions. This model of RoboMet.3D system can use up to 8 grinding/polishing pads and 5 different polishing fluids to sequentially remove material from the sample-of-interest, while producing a surface appropriate for materialographic analysis.

Sample Preparation for RoboMet.3D

The RoboMet.3D sample holder used for this study can accommodate up to a 1.5 in. dia. materialographic mount, which required machining of the 6 x 4 in. panels before mounting. Also, the typical maximum depth of a serial sectioning experiment is approximately 10 mm, which corresponds to the range of the motorized focus drive on the optical microscope. Using the correlative UT and digital camera data described in the previous section, the extent of the damage region was marked on the plate surface using a permanent marker to simplify sectioning of the panel using a slow-speed diamond saw. For specimen D3-6, the damage region was sufficiently small, permitting inclusion of the entire damage region in the serial sectioning sample. For specimen D3-5, the damage region diameter exceeded the 10 mm maximum depth of the serial sectioning experiment. Consequently, the damage area was sectioned in half, as shown in the schematic in Fig. 6. The specimens were cut using a slow-speed water-lubricated diamond saw. After sectioning, the PMC samples were cast into a 1.25 in. diameter cylindrical mount using epoxy resin suitable for materialographic sectioning (Buehler EpoThin).

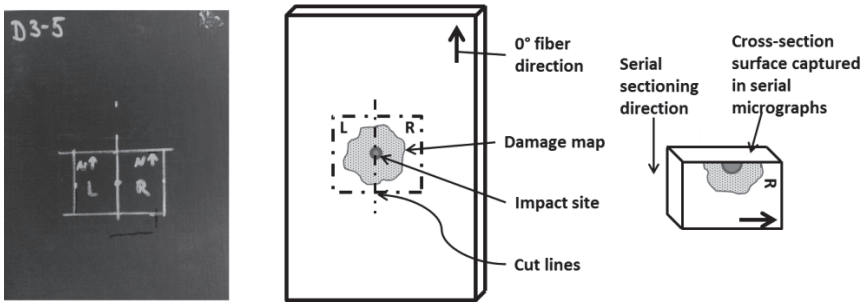

FIGURE 6. Photograph and schematic of sample preparation for specimen D3-5.

Serial Sectioning Parameters

An important aspect of serial sectioning experiments is to balance the requirements of sufficient resolution and volumetric coverage to characterize the microstructural features of interest, with the potentially exponential increases in time associated with increasing spatial resolution and volume examined. For the two experiments described in this study, the average serial section thickness (spacing between consecutive sections) was 6.7 and 23 micrometers, while the in-plane resolution for the optical microscope data was 0.52 and 0.67 micrometers. Relative to typical serial sectioning experiments, the ratio of in-plane resolution to serial section thickness is much larger, here, a factor of 13 and 34 compared to typical values of 0.5 to 5. As a result, visualization and feature identification in these data sets contain artifacts, as current algorithms for classifying features in 3D rely on having nearest-neighbor voxel connectivity.

TABLE 3. Serial sectioning parameters for impact damage characterization studies

Parameter	Specimen D3-6 (2.7 Joule)	Specimen D3-5 (4.3 Joule)
Number of Sections	454	80
Number of Image Tiles per Section	40 (8 x 5, 20% Overlap)	231 (33 x 7, 10% Overlap)
Optical Montage Pixel Resolution	0.519 μm/pixel (20x, 1.0 Optivar, 0.4 NA)	0.669 μm/pixel (10x, 1.6 Optivar, 0.2 NA)
Optical Montage Field-of-View	8.4 x 4.0 mm	24.9 x 3.45 mm
Average Serial Section Thickness	6.7 μm/slice	23.3 μm/slice
Total Serial Section Thickness	3018 mm	2061 mm
Serial Section Volume	101 mm^3	177 mm^3
Serial Section Image Data	30.9 GB	14.1 GB
Cycle Time per Section	40:30 (35:10 Prep/5:20 Image)	52:45 (39:50 Prep/12:55 Image)
Collection Time	12 days, 19 hours	2 days, 23 hours

While the general procedure is similar for both serial sectioning experiments as shown in Table 3, there were minor modifications between the two experiments to maximize data quality while minimizing total experiment time. For both samples, the material removal step was accomplished using a series of polishing steps, starting with 15 micrometer diamond abrasive, followed by 6 micrometer and 1 micrometer diamond abrasive, using Struers DAC polishing pads. Between polishing steps, the sample was cleaned using a soft pad (Allied Final Pol) with flowing tap water to remove the diamond media from the previous step. Before optical microscopy, the sample surface was immersed in ultrasonic cleaner filled with pure Ethanol and sonicated for 15 seconds, followed by drying using a Nitrogen gas stream.

Optical image acquisition was performed using a Zeiss Axiovert 200M inverted optical microscope outfitted with an MRc5 camera, and Zeiss AxioVision software was used for automated montage image capture. Bright-field reflection imaging conditions were used to illuminate the as-polished surfaces, and the overlap between adjacent images in the montage array was prescribed at 10%. The magnification lens selections for the two experiments were slightly different. The experiment on the Panel D3-6 utilized a Zeiss AxioPlan 20X, 0.4 NA objective lens with a 1.0 Optivar, resulting in a sampling (pixel) resolution of 0.519 micrometers, while the Panel D3-5 utilized a Zeiss AxioPlan 10x, 0.2 NA objective lens with a 1.6 Optivar lens combination for a sampling resolution of 0.669 micrometers. In both experiments, 12-bit monochrome images were collected.

Post-processing and Analysis of Optical Image Data

Next, optical image data from the serial sectioning experiments was post-processed to create 3D data sets. First, illumination non-uniformities due to the set-up of the optical microscope were removed by calculating a normalized average image from the respective sets of optical image data (so-called retrospective flatfielding [9]), and dividing each image tile by the calculated background image. The image tiles from each section of the experiment were then fused into a single composite image, a.k.a. montage image, using the "Grid/Collection Stitching Plug-In" for ImageJ

[10], which utilizes normalized phase cross correlation and an iterative optimization procedure to minimize cumulative errors in tile displacements. For example, in the experiment on panel D3-5, 231 images were fused to create a single montage image that contained ~37,200 x 5000 pixels with a 0.667 micrometer pixel resolution, corresponding to a field of view of 24.8 x 3.4 mm. The stack of montage images were aligned and registered using the "Linear Stack Alignment with SIFT Plug-In" for ImageJ [10], using only translations.

For segmentation of the delaminations and matrix cracks, this operation was performed using an intensity threshold. The threshold was determined through analysis of the image histogram, and a representative image and its associated histogram are shown in Fig. 7. The reflected light intensities of cracks, delaminations, and pores are at low values and well separated from other key features in the optical image data, such as the polymer matrix (medium intensity levels), and the carbon fibers (high intensity levels), as shown in the histogram on the right side of Fig. 7. The threshold was determined as the intensity value equidistant between the modes of the intensity distributions for cracks/delaminations and the polymer matrix.

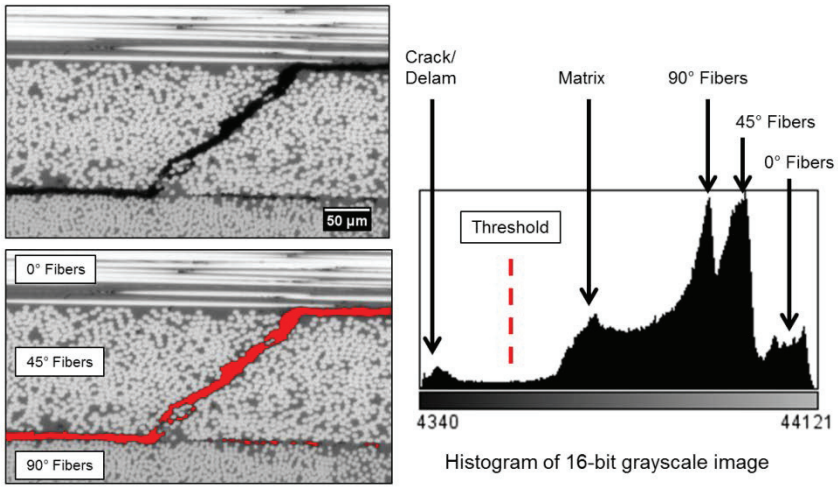

FIGURE 7. Micrograph before and after threshold segmentation for cracks/delaminations, along with the associated histogram that denotes selected intensities associated with key features in the optical image.

RESULTS AND ANALYSIS

The remainder of this paper will focus on results, analysis, and conclusions drawn from specimen D3-5, as the data produced and analyzed for specimen D3-6 are thus far inconclusive. Ply interfaces will be referenced according to the legend in Table 4. The numbering sequence is referenced from the impacted surface of the panel ("top" surface) and increases through-the-thickness of the panel until reaching the back surface. "Interface 0" and "Interface 24" would indicate the top and back surface of the panel, respectively, but will be referred to by "top surface" or "front wall," and "back surface" or "back wall" to distinguish from inter-ply interfaces.

TABLE 4. Reference to ply interface nomenclature for $[-45/90/45/0]_{3S}$ stacking sequence

Ply Interface	**-45/90**	**90/45**	**45/0**	**0/-45**	**-45/90**	**90/45**	**45/0**	**0/-45**	**-45/90**	**90/45**	**45/0**	**0/0**
Intfc #	1	2	3	4	5	6	7	8	9	10	11	12
Ply Interface	**0/45**	**45/90**	**90/-45**	**-45/0**	**0/45**	**45/90**	**90/-45**	**-45/0**	**0/45**	**45/90**	**90/-45**	
Intfc #	13	14	15	16	17	18	19	20	21	22	23	

Ultrasonic Testing Delamination Characterization

High-resolution UT scan results were post-processed to produce interface-by-interface C-scans. The speed of sound in the material was calculated using measured specimen thickness and through-thickness time-of-flight. Nominal ply thickness was calculated using the known number of plies in the laminate and the measured specimen thickness. Then, ultrasound reflections at every ply interface were identified by simultaneously analyzing maximum amplitude and time-of-flight C-scans with selected A-scans. To enable the per-interface analysis, time gates were used to isolate each interface, and those C-scans were saved for further analysis as shown in Fig. 8.

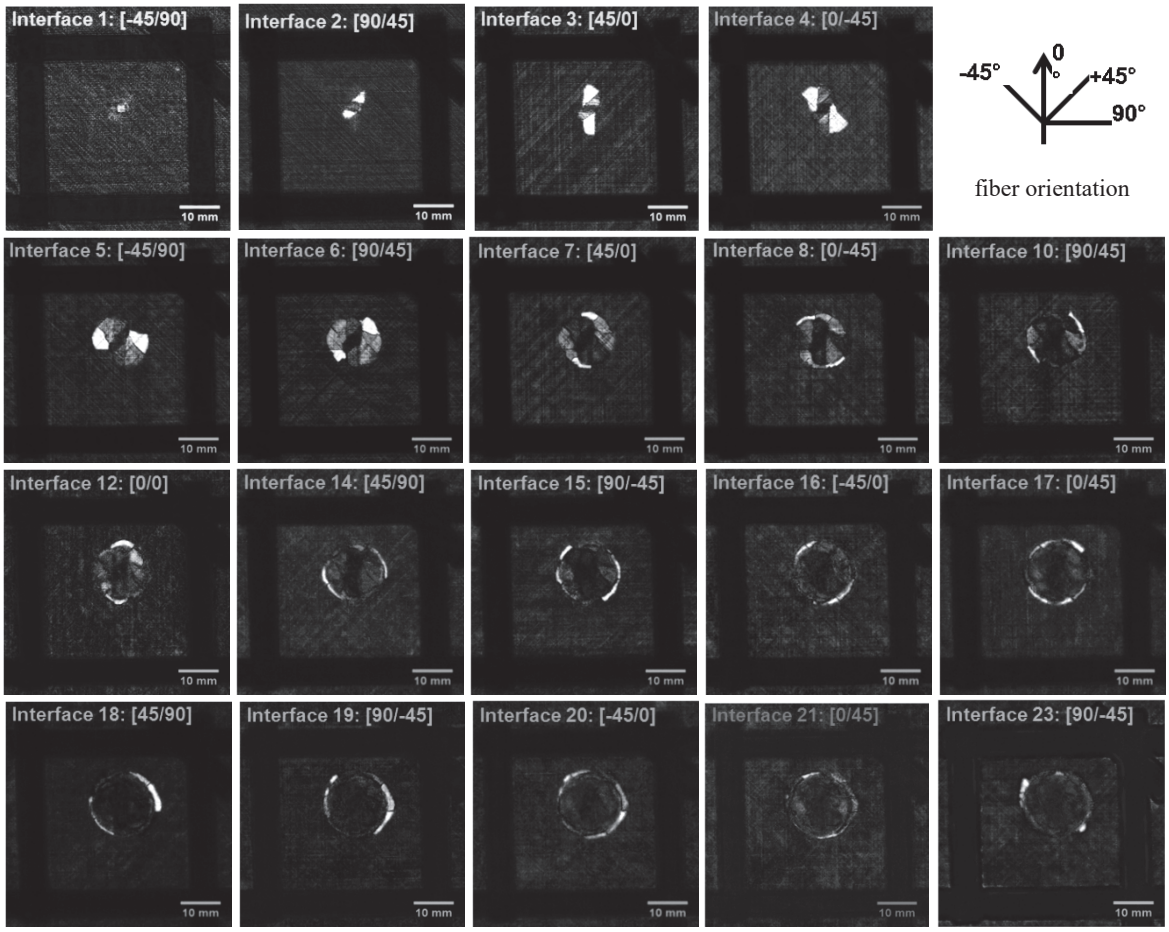

FIGURE 8. Subset of specimen D3-5, maximum amplitude UT C-scans, time-gated at ply interfaces.

Qualitative analysis of the interface-by-interface UT C-scans highlights two main features of the delamination morphology. First, delamination shape and orientation are clearly linked to the laminate ply fiber direction and stacking sequence, which is consistent with previously published work by Aymerich et al. [11] and Sebaey et al. [12, 13]. The C-scan data show nominal delamination shapes of elongated "pie-wedge" shaped sectors, where the edges of wedge-shaped delaminations are correlated to the fiber directions of the plies that compose each interface. In addition, there is a 45° rotation of the overall orientation of these wedge-shaped delaminations between successive plies, shown most clearly in Fig. 8 at interfaces 2-5.

Second, as previously reported [11-13], it is readily apparent that characterization of all inter-laminar delaminations is not possible using only a normal-incidence, pulse-echo, single-sided UT scan. The delaminations that are very near the impact surface are readily observed; however, delaminations in other ply interfaces that directly beneath another delamination are effectively shielded and are unable to be interrogated using this scanning procedure. Nonetheless, delaminations that extend beyond the area of the near-surface delaminations can be located and characterized, and for this particular sample, it appears that delaminations are progressively larger in radial size

through the thickness of the panel. We note that impact-induced delamination patterns and features are dependent on laminate stacking sequence and other parameters, as discussed in [12, 13].

Serial Section Delamination Characterization

A preliminary analysis was performed to demonstrate that the serial sectioning measurements provided high resolution detail on the delamination and matrix crack morphology below the impact site. As shown in Fig. 9, the threshold segmentation described previously provided a detailed representation of the complex cracking below the impact site, including "shadowed" delaminations that were not observable in the UT data. The longest interlaminar delaminations in this particular subvolume are associated with [45/0] interfaces above the [0/0] symmetry interface, and [-45/0] interfaces below the symmetry interface. The total spans (end-to-end distances that span the entire impact site) of these longest delaminations were measured using ImageJ, and, these values are listed in Table 5. These measurements are in qualitative agreement with the maximum amplitude C-scan data shown in Fig. 8, where the shortest delaminations are for the interfaces closest to the impact surface, and the delaminations grow progressively larger with depth away from the impact.

In addition, for the volume examined, one can observe that selective delaminations at adjacent ply interfaces are connected by transverse matrix cracks throughout the impact site. For the volume of material that was characterized, matrix cracks are observed near or at the inner or outer edges of selected delaminations, and, are only observed to propagate through one ply layer, although there may be multiple matrix cracks in close proximity. Also, ~ 1 mm dia. cylindrical region of material centered on the impact site does not appear to contain any significant damage.

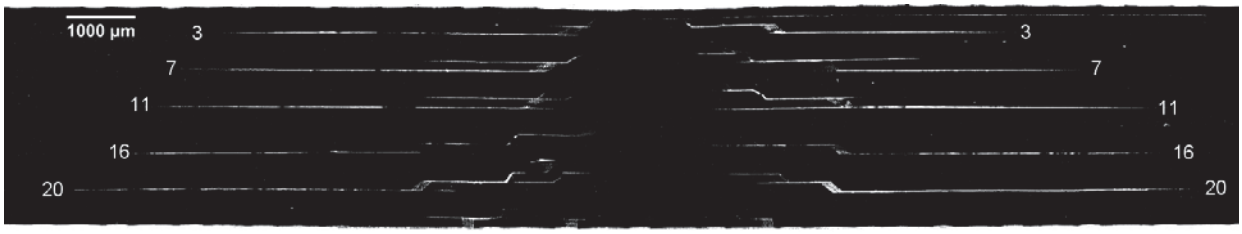

FIGURE 9. Threshold image from the serial sectioning data, highlighting the delamination and matrix crack substructure contained within the serial sectioning volume for specimen D3-5.

TABLE 5. Measurement of Delamination Span from Optical Microscopy Data

Interface Delamination ID	Total Span of Delamination (mm)
3 [45/0]	11.2 ± 0.1
7 [45/0]	12.6 ± 0.1
11 [45/0]	14.2 ± 0.1
16 [-45/0]	14.3 ± 0.1
20 [-45/0]	15.8 ± 0.1

CONCLUSIONS AND FUTURE WORK

A correlative study using both normal incidence ultrasonic testing and mechanical polishing serial sectioning has been presented to characterize the delamination substructure associated with barely visible impact damage in polymer matrix composite laminate panels. This approach has the potential to significantly improve the quantitative measurement of the subsurface damage field using ultrasonic scans, as, modern serial sectioning microscopy methods can provide sub-micrometer resolution data over cm-scale volumes on both the delaminations and matrix cracks associated with low energy (< 5 J) instrumented impact tests.

Future work includes quantitative comparison of the delamination substructure in 3D from both UT and serial sectioning characterization. This requires a number of advancements beyond the present study, including improved experimental and computational methods to simplify the spatial registration of the two data modalities. Additional serial sectioning characterization of an entire impact damage region is desired, with selection of a sectioning plane

that is at an oblique angle to the fiber direction for all ply orientations, and, utilizing a finer sectioning thickness to enable accurate 3D reconstruction of the damage structure.

ACKNOWLEDGMENTS

The authors would like to acknowledge the valuable contributions made to this work by Dr. Michael Chapman (UES, Inc.), David Zainey (University of Dayton Research Institute), and Josiah Dierken (University of Dayton Research Institute). Michael led the execution of serial sectioning experiments and assisted with image post-processing of the materialographic data set. David was instrumental in set-up and operation of the MaPSS II system for acquisition of the hi-resolution ultrasound data sets. Josiah performed the critical image registration step of UT C-scan to optical image of the specimen panel. The work of these contributors was funded by the Air Force Research Laboratory, Materials and Manufacturing Directorate, Wright-Patterson Air Force Base, Ohio.

REFERENCES

1. E. Lindgren, D. Mollenhauer, M. Flores, S. Wallentine, J. Welter, "Damage Tolerance for Life Management of Composite Structures – Part 2: Nondestructive Evaluation," *Aircraft Structural Integrity Program Conference*, (2015).
2. D. Mollenhauer, E. Iarve, K. Hoos, M. Flores, E. Zhou, E. Lindgren, and G. Schoeppner, "Damage Tolerance for Life Management of Composite Structures – Part 1: Modeling," *Aircraft Structural Integrity Program Conference*, (2015).
3. J. Wertz, S. Wallentine, J. Welter, J. Dierken, and J. Aldrin, "Volumetric Characterization of Delamination Fields via Angle Longitudinal Wave Ultrasound," *Review of Progress in Quantitative Nondestructive Evaluation*, 36, (eds.) D. E. Chimenti and L. J. Bond, **1806**, 090006, (2017).
4. M. Uchic, M. Groeber, "An Automated Multi-Modal Serial Sectioning System for Characterization of Grain-Scale Microstructures in Engineering Materials,"*1 International Conference on 3D Materials Science*, (eds.) M. De Graef, H. F. Poulsen, pp. 195-202, (2012).
5. M. Groeber and M. Jackson, "DREAM.3D: A Digital Representation Environment for the Analysis of Microstructure in 3D," *Integrating Materials and Manufacturing Innovation,* **3:**5, 17 pp. (2014).
6. ASTM D7136/D7136M-15, Standard Test Method for Measuring the Damage Resistance of a Fiber-Reinforced Polymer Matrix Composite to a Drop-Weight Impact Event, *ASTM International*, (2015).
7. M. Flores, D. Mollenhauer, "High-speed digital image correlation of low-velocity impacts on composite plates," *Composites Part B,* **131**, 153-164, (2017).
8. G.A. Schoeppner, S. Abrate, "Delamination threshold loads for low velocity impact on composite laminates," *Composites Part A,* **31**, 903-915, (2000).
9. Likar, Maintz, Viergever and Pernuš, "Retrospective shading correction based on entropy minimization," *Journal of Microscopy,* **197**, 285-295, (2000).
10. Schindelin, J, Arganda-Carreras, I. and Frise, E. "Fiji: an open-source platform for biological-image analysis," *Nature methods,* **9**:7, 676-682, (2012).
11. F. Aymerich, S. Meili, "Ultrasonic evaluation of matrix damage in impacted composite laminates," *Composites Part B,* **31**, 1-6, (2000).
12. T.A. Sebaey, E.V. Gonzalez, "Damage resistance and damage tolerance of dispersed CFRP laminates: Effect of the mismatch angle between plies," *Composite Structures,* **101**, 255-264, (2013).
13. T.A. Sebaey, E.V. Gonzalez, "Damage resistance and damage tolerance of dispersed CFRP laminates: Effect of ply clustering," *Composite Structures,* **106**, 96-103, (2013).